

Microwave shielding of ultracold polar molecules with imperfectly circular polarization

Tijs Karman* and Jeremy M. Hutson

*Joint Quantum Centre (JQC) Durham-Newcastle, Department of Chemistry,
Durham University, South Road, Durham, DH1 3LE, United Kingdom*

(Dated: August 26, 2022)

We investigate the use of microwave radiation to produce a repulsive shield between pairs of ultracold polar molecules and prevent collisional losses that occur when molecular pairs reach short range. We carry out coupled-channels calculations on RbCs+RbCs and CaF+CaF collisions in microwave fields. We show that effective shielding requires predominantly circular polarization, but can still be achieved with elliptical polarization that is around 90% circular.

I. INTRODUCTION

Ultracold polar molecules provide many new opportunities for quantum science, and may in future provide a new platform for quantum technology. Several groups have succeeded in producing samples of such molecules, either by direct laser cooling of preexisting molecules [1, 2] or by associating pairs of ultracold atoms and transferring the resulting weakly bound molecules to the ground state [3–10].

A few groups have carried out experiments on collisions of ultracold polar molecules. Fermionic molecules in identical states are protected against collisions at the lowest temperatures [9, 11], but all bosonic species investigated so far have been found to undergo fast collisional trap loss. The same is true for fermionic molecules in different internal states. For some molecules, such as KRb [11], the loss may be attributed to energetically allowed 2-body reactions. However, fast loss with second-order kinetics appears to exist [12, 13] even when there are no energetically allowed 2-body pathways [14]. In such cases the loss may be mediated by formation of long-lived collision complexes, followed by either collision with a third molecule [15] or excitation by the trapping laser [16, 17].

It thus appears that active measures are needed to stabilize gases of ultracold polar molecules against collisions. An appealing possibility is microwave shielding with blue-detuned microwave radiation [18, 19], which provides a repulsive shield that prevents the molecules coming close together. We have recently shown that such shielding can be achieved with circularly polarized microwaves at high Rabi frequencies, but not with linearly polarized microwaves [19].

Pure circular polarization is hard to achieve for microwaves at the frequencies and intensities needed for shielding. In this paper we explore the effect of imperfectly circular polarization and show that good shielding can be achieved with elliptical polarization that is around 90% circular.

II. THEORY

The calculations carried out in the present paper use an extension of the methods described in Ref. [19]. We consider a collision between two polar molecules, each dressed with microwave radiation that is blue-detuned by Δ from its $n = 0 \rightarrow 1$ rotational transition. The intensity of the microwave radiation is specified by the Rabi frequency Ω .

Our basic physical picture is that two molecules interact at long range via the dipole-dipole interaction. In the presence of blue-detuned microwave radiation, this provides a repulsive shield. Under conditions where shielding is effective, most molecules are reflected at long range, and do not approach each other close enough for short-range processes to occur. There are nevertheless two processes that can cause loss. First, any colliding pairs that do reach short range are usually lost. Secondly, even pairs that are reflected at long range may undergo inelastic transitions to lower-lying field-dressed states. These transfer internal energy into relative kinetic energy and generally eject both collision partners from the trap. We refer to this latter process as microwave-induced loss.

To model shielding and loss, we carry out coupled-channels scattering calculations. We propagate two sets of linearly independent solutions of the coupled-channels equations, using the renormalized Numerov method [20], and apply both capture boundary conditions at short range and S -matrix boundary conditions at long range [21–23]. We calculate both the probability of reaching short range (RSR) and the rate coefficient for microwave-induced loss. The remaining flux is shielded and scatters elastically.

The molecules are modeled as rigid rotors with a dipole moment. The monomer Hamiltonian of molecule X is

$$\hat{H}^{(X)} = b_{\text{rot}} \hat{n}^2 + \hat{H}_{\text{hyperfine}}^{(X)} + \hat{H}_{\text{ac}}^{(X)}. \quad (1)$$

The first term describes the rotational kinetic energy, with rotational constant b_{rot} . The second term describes the molecular hyperfine Hamiltonian, and is discussed in the Supplement of Ref. [19]. The last term represents the

* Present address: ITAMP, Harvard-Smithsonian Center for Astrophysics, Cambridge, MA, 02138, USA

interaction with a microwave electric field [24],

$$\hat{H}_{\text{ac}}^{(X)} = -\frac{E_{\text{ac}}}{\sqrt{N_0}} \left[\hat{\mu}_{\sigma}^{(X)} \hat{a}_{\sigma} + \hat{\mu}_{\sigma}^{(X)\dagger} \hat{a}_{\sigma}^{\dagger} \right] + \hbar\omega \hat{a}_{\sigma}^{\dagger} \hat{a}_{\sigma}. \quad (2)$$

The microwave electric field strength is given by E_{ac} , and N_0 is the reference number of photons. The operators $\hat{a}_{\sigma}^{\dagger}$ and \hat{a}_{σ} are creation and annihilation operators for photons in polarization mode σ and angular frequency ω . The polarization may be linear, with Cartesian components $\sigma = x, y$, and/or z , circular, with spherical components $\sigma = \pm 1$ and $\hat{\mu}_{\pm 1}^{(X)} = \mp (\hat{\mu}_x^{(X)} \pm i\hat{\mu}_y^{(X)})/\sqrt{2}$, or elliptical. A general elliptical polarization in the xy plane can be described as

$$\sigma_{\xi} = \sigma_{+} \cos \xi - \sigma_{-} \sin \xi. \quad (3)$$

The ellipticity angle ξ interpolates between pure σ_{+} polarization at $\xi = 0$ and linear σ_x polarization at $\xi = \pi/4$. The form of the interaction with a microwave electric field, Eq. (2), remains valid with $\hat{\mu}_{\xi} = \hat{\mu}_{+1} \cos \xi - \hat{\mu}_{-1} \sin \xi$.

The total Hamiltonian is

$$\hat{H} = -\frac{\hbar^2}{2M} \frac{1}{R} \frac{d^2}{dR^2} R + \frac{\hbar^2 \hat{L}^2}{2MR^2} + \hat{H}^{(A)} + \hat{H}^{(B)} + \hat{V}(R). \quad (4)$$

Here M is the reduced mass, R is the distance between the molecules and \hat{L} is the dimensionless angular momentum operator associated with the end-over-end rotation of the intermolecular axis, \vec{R} . The first term describes the radial kinetic energy and the second the centrifugal kinetic energy. The third and fourth terms correspond to the monomer Hamiltonian of Eq. (2). The final term is the interaction potential $\hat{V}(R)$, which in the present work is limited to the dipole-dipole interaction [19],

$$\hat{V}(R) = -\frac{\sqrt{6}}{4\pi\epsilon_0 R^3} T^{(2)}(\hat{\mu}^{(A)}, \hat{\mu}^{(A)}) \cdot C^{(2)}(\hat{R}). \quad (5)$$

We use completely uncoupled basis sets. The basis set for monomer $X = A, B$ consists of products of rotational, spin and photon states,

$$|n_X m_{n_X}\rangle |i_X m_{i_X}\rangle |N\rangle, \quad (6)$$

where $|i_X m_{i_X}\rangle$ schematically represents all the spins on molecule X ; it may be a product of spin functions, including electron spin where necessary. The number of photons with polarization σ and detuning Δ is $N + N_0$, where $N_0 \gg 1$ is the reference number of photons. For the colliding pair of molecules we introduce an angular momentum state, $|LM_L\rangle$, that describes the end-over-end rotation of the intermolecular axis. The basis functions for the pair of molecules are [25–27]

$$|n_A m_{n_A}\rangle |i_A m_{i_A}\rangle |n_B m_{n_B}\rangle |i_B m_{i_B}\rangle |LM_L\rangle |N\rangle. \quad (7)$$

Only even values of L are included: The only interaction that couples states with different L is the dipole-dipole

interaction, and this conserves the parity of L . The basis functions are adapted to permutation symmetry as described in the Supplement of Ref. [19].

Excluding the photons, the direct-product basis functions have a well-defined projection quantum number M_{tot} for the projection of the total angular momentum along the space-fixed z axis,

$$M_{\text{tot}} = m_{n_A} + m_{i_A} + m_{n_B} + m_{i_B} + M_L. \quad (8)$$

For linear z or circular $x \pm iy$ polarizations, with $\sigma = 0, \pm 1$, the generalized projection quantum number \mathcal{M} is conserved,

$$\mathcal{M} = M_{\text{tot}} + \sigma N, \quad (9)$$

and the basis set can be limited to include only functions with a single value of \mathcal{M} . For elliptical polarization in the xy plane, however, there is no generalized projection quantum number that is conserved. In this case, the basis set must include functions with various values of \mathcal{M} , and the calculation is correspondingly more computer intensive.

We showed in Ref. [19] that molecular fine and hyperfine interactions cause an increase in microwave-induced loss at zero magnetic field, but that the increase can be suppressed by applying a moderate magnetic field perpendicular to the plane of polarization. We demonstrate in the Supplemental Material that the field required to suppress the effects of hyperfine interactions is proportional to the ratio of the hyperfine constants to the nuclear g-factors. For molecules in $^2\Sigma$ states, the field needed is proportional to the ratio of the spin-rotation constant to the electron g-factor. Since there is a tendency for both hyperfine coupling constants and nuclear g-factors to increase with atomic number, the magnetic field required to suppress hyperfine effects does not vary enormously, and is typically on the order of 100 G. The key issue is that the magnetic field must be high enough that m_n is nearly conserved. When it is, the microwave-induced loss for the bialkalies is reduced to the hyperfine-free level, while that for molecules in $^2\Sigma$ states is incompletely suppressed [28].

III. RESULTS

We have carried out coupled-channel calculations for RbCs+RbCs and CaF+CaF collisions in microwave fields, with the molecules in their ground electronic states, $X^1\Sigma^+$ and $X^2\Sigma^+$, respectively. The calculations used $n_{\text{max}} = 1$, $L_{\text{max}} = 6$, $N = 0, -1, -2$, and a collision energy of 1 μK . Electron and nuclear spins were not included explicitly, but for CaF the calculation included spin-dependent couplings averaged over the spin-stretched state. As shown in the Supplemental Material, these calculations are appropriate for magnetic fields above 100 G [28].

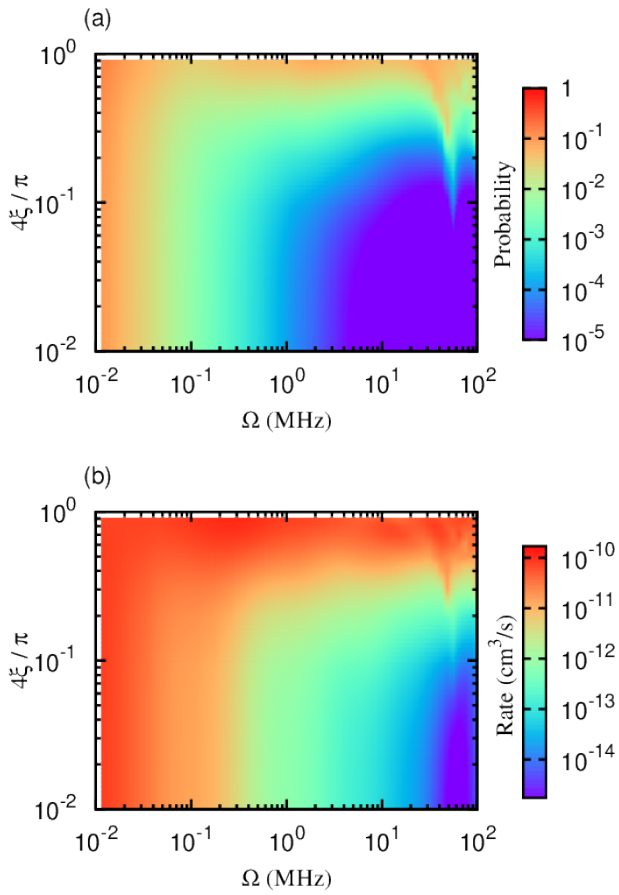


Figure 1. Probability of RSR (a) and rate coefficient for microwave-induced loss (b) in RbCs+RbCs collisions with microwave detuning $\Delta = 0$, as a function of Rabi frequency, Ω , and ellipticity angle, ξ .

Figure 1 shows the probability of RSR and the rate coefficient for microwave-induced loss for RbCs as a function of the ellipticity angle, ξ , and the Rabi frequency, Ω , for fixed $\Delta = 0$. At the top of the figures, where $4\xi/\pi \approx 1$, the probability of RSR and the microwave-induced loss rate are both large. This corresponds to linear polarization, for which shielding is ineffective. At the bottom of the figure, below $4\xi/\pi \approx 0.01$, the probability of RSR and the microwave-induced loss rate become independent of ξ and visually indistinguishable from the result for circular polarization. Losses can be suppressed to four orders of magnitude below the universal loss rate [29], which for RbCs at zero energy is $1.7 \times 10^{-10} \text{ cm}^3 \text{ s}^{-1}$. These values of ξ correspond to an impurity in the microwave polarization of less than 1 %, which may be experimentally realizable. An ellipticity of up to 10 %, corresponding to $4\xi/\pi \approx 0.1$, results in somewhat increased losses but still provides effective shielding.

Figure 2 shows the probability of RSR and the rate coefficient for microwave-induced rate for CaF as a function of the ellipticity angle, ξ , and the Rabi frequency,

Ω , for fixed $\Delta = 0$. The spin degrees of freedom are not explicitly accounted for, but the calculation includes fine and hyperfine couplings averaged over the spin-stretched state, which is appropriate for magnetic fields above 100 G [28]. The resulting couplings increase the microwave-induced loss. The resulting shielding is less effective than for RbCs, but the losses are still reduced by up to three orders of magnitude from the universal loss rate of $5 \times 10^{-10} \text{ cm}^3 \text{ s}^{-1}$. The loss rates are essentially indistinguishable from those for circular polarization for $4\xi/\pi \leq 0.1$, corresponding to an imperfection from circular polarization of 10 %.

IV. FIXED- θ COLLISIONS (SUDDEN APPROXIMATION)

To understand the way that the losses depend on the ellipticity angle, we consider a sudden approximation in which the orientation of the intermolecular axis is assumed to remain constant during a collision. The ori-

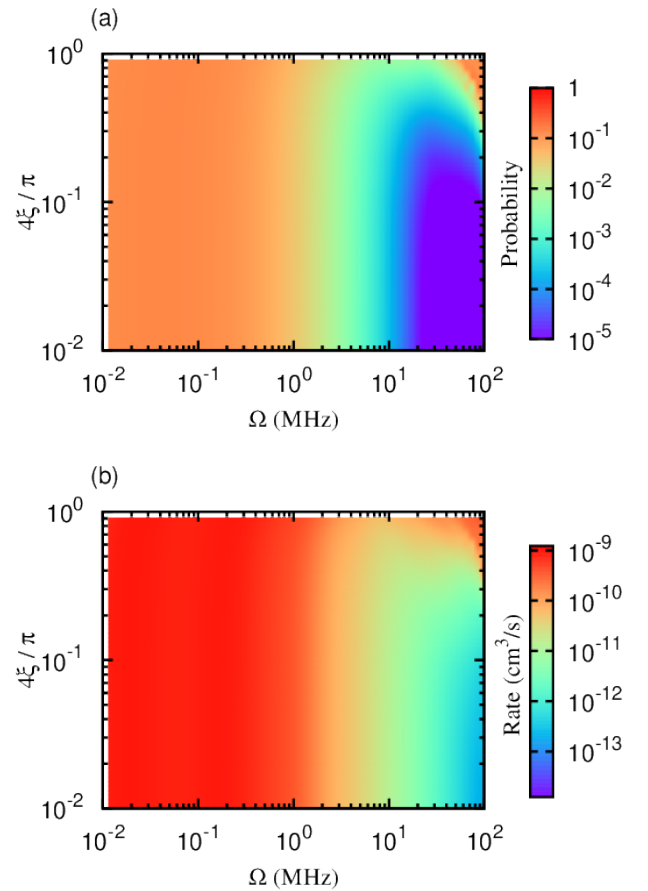


Figure 2. Probability of RSR (a) and rate coefficient for microwave-induced loss (b) in CaF+CaF collisions with microwave detuning $\Delta = 0$, as a function of Rabi frequency, Ω , and ellipticity angle, ξ .

tation is specified by the polar angles (θ, ϕ) of \hat{R} with respect to the space-fixed frame. The spherical harmonics $|L, M_L\rangle$ are dropped from the basis set. This approximation is expected to be accurate if the period of an end-over-end rotation of the complex is long compared to the duration of a collision, which may not be the case. It also neglects nonadiabatic losses due to couplings involving $d/d\theta$, which may be significant. The fixed- θ approximation is therefore not quantitatively accurate, but it nevertheless provides useful insights.

Figure 3 shows adiabatic potential curves for RbCs+RbCs, defined as eigenvalues of the pair Hamiltonian, Eq. (4), excluding radial kinetic energy, as a function of R for fixed θ . This representation is much simpler than is obtained by diagonalizing in the full basis set that includes the dependence on θ through the partial-wave expansion, as shown in Fig. 3 of the Supplement of Ref. [19]. Figure 3 provides a less crowded representation of the adiabats that removes many of the inconsequential crossings of low and high- L states corresponding to different thresholds. In each case the colliding molecules are initially at the uppermost of the thresholds shown.

The upper two panels of Figure 3 show adiabats for the off-resonant case, $\Omega \ll \Delta$. This is not the parameter regime in which effective shielding is realized, but the potential curves are more easily understood. In this case the ground-state ($|n_A, n_B, N\rangle = |0, 0, 0\rangle$) and microwave-dressed excited-state ($|0, 1, -1\rangle$) potentials are essentially unmodified by the microwaves. The ground-state (upper) potential is determined by rotational dispersion and varies with R^{-6} . The excited-state (lower) potential is split by resonant dipole-dipole interactions into an attractive and repulsive branch, which vary with R^{-3} ; the attractive branch is mostly off scale in Fig. 3. Resonant dipole-dipole interactions quantize the rotational angular momentum along the intermolecular axis with projection quantum number K , giving potentials that are independent of orientation with respect to the microwave polarization: $K = 0$ for the attractive branch and $K = \pm 1$ for the repulsive branch. In this off-resonance scenario, coupling by the microwaves is significant only near the point where the ground-state potential crosses the repulsive $K = \pm 1$ branch of the excited state, around $800 a_0$ in Fig. 3. For linear π or circular σ_{\pm} polarization, the microwave field couples the ground state to the excited state with well-defined space-fixed projection quantum number $M_N = m_{nA} + m_{nB} = 0$ or ± 1 , respectively. Hence, the coupling to the repulsive $K = \pm 1$ branch depends on the polar angle of the intermolecular axis, θ , as the Wigner d -function $d_{M_N, K}^{(1)}(\theta)$. For circular σ_{\pm} polarization, shown in Fig. 3(a), the crossing is avoided for all angles θ , although the degree of avoidedness is anisotropic and varies with $\sqrt{1 + \cos^2 \theta}$. For linear π polarization, shown in Fig. 3(b), the avoidedness of the crossing varies with $\sin \theta$, and vanishes at $\theta = 0$. This implies that there is a “hole” in the shielding at $\theta = 0$ with linear polarization.

Next, we consider the resonant case, $\Omega \gg \Delta = 0$,

where effective shielding is achieved with near-circular polarization. The adiabats are shown in the lower two panels of Figure 3. Here, there is strong dressing that mixes the $n = 0$ ground and $n = 1$ excited states even for the isolated molecules. This can be interpreted as inducing an oscillating dipole moment in the lab frame, which produces first-order dipole-dipole interactions upon time averaging. As a result, the adiabats vary with $R^{-3}P_2(\cos \theta)$ at long range. The space-fixed dipole-dipole interactions are attractive for some orientations, i.e., near $\theta = 0$ for linear π polarization and near $\theta = \pi/2$ for circular σ_{\pm} polarization. However, at shorter separation, the dipole-dipole interaction becomes stronger than $\hbar\Omega$, and this interaction again quantizes the molecules along the intermolecular axis, such that the top adiabatic curve is repulsive for all θ . As discussed above, the coupling from the initial state to this repulsive branch depends on θ . For circular polarization, shown in Fig. 3(c), the angle dependence is again such that the coupling to the repulsive branch never vanishes. For linear polarization, shown in Fig. 3(d), the shielding again vanishes at $\theta = 0$, where both $K = \pm 1$ repulsive states are uncoupled from the initial state. For small θ , this leads to a narrowly avoided crossing between the initial state and the lower field-dressed level; this occurs outside the repulsive shield and is classically accessible. As a result, linear polarization does not achieve shielding, but it does give rise to additional microwave-induced losses. For imperfectly circular polarization, the effective coupling to the repulsive branch is reduced from that for circular polarization, but does not vanish.

It is worth noting that the space-fixed dipole-dipole interaction discussed here produces attractive interactions outside the repulsive shield. Where these support bound states, they can be used to tune the scattering length while shielding from short-range losses, as shown in Ref. [30].

We next carry out coupled-channels calculation of shielding and loss in the fixed- θ approximation. For these we consider elliptical polarization in the xy plane, with $\xi = \pi/4$ corresponding to linear polarization along x (σ_x polarization). This differs from the discussion above, which considered linear polarization along z (π polarization). Since only the microwave polarization defines a preferential direction, this choice is inconsequential, but it does mean that collisions now occur along the axis of linear polarization when $\theta = 90^\circ$ rather than $\theta = 0$.

Figure 4 shows the probabilities of RSR and the rate coefficients for microwave-induced loss in RbCs+RbCs collisions, for $\Delta = 0$, as a function of the Rabi frequency, Ω , and the fixed angle, θ , between the intermolecular axis and microwave propagation direction. The three rows correspond to different polarizations: σ_+ , σ_x , and elliptical polarization with $\xi = 0.2\pi/4$. For circular polarization, shown in the top row, we find both types of loss can be suppressed by using sufficiently high Rabi frequency. The loss is highest for $\theta = \pi/2$, where coupling to the repulsive branch of the resonant dipole-dipole interaction

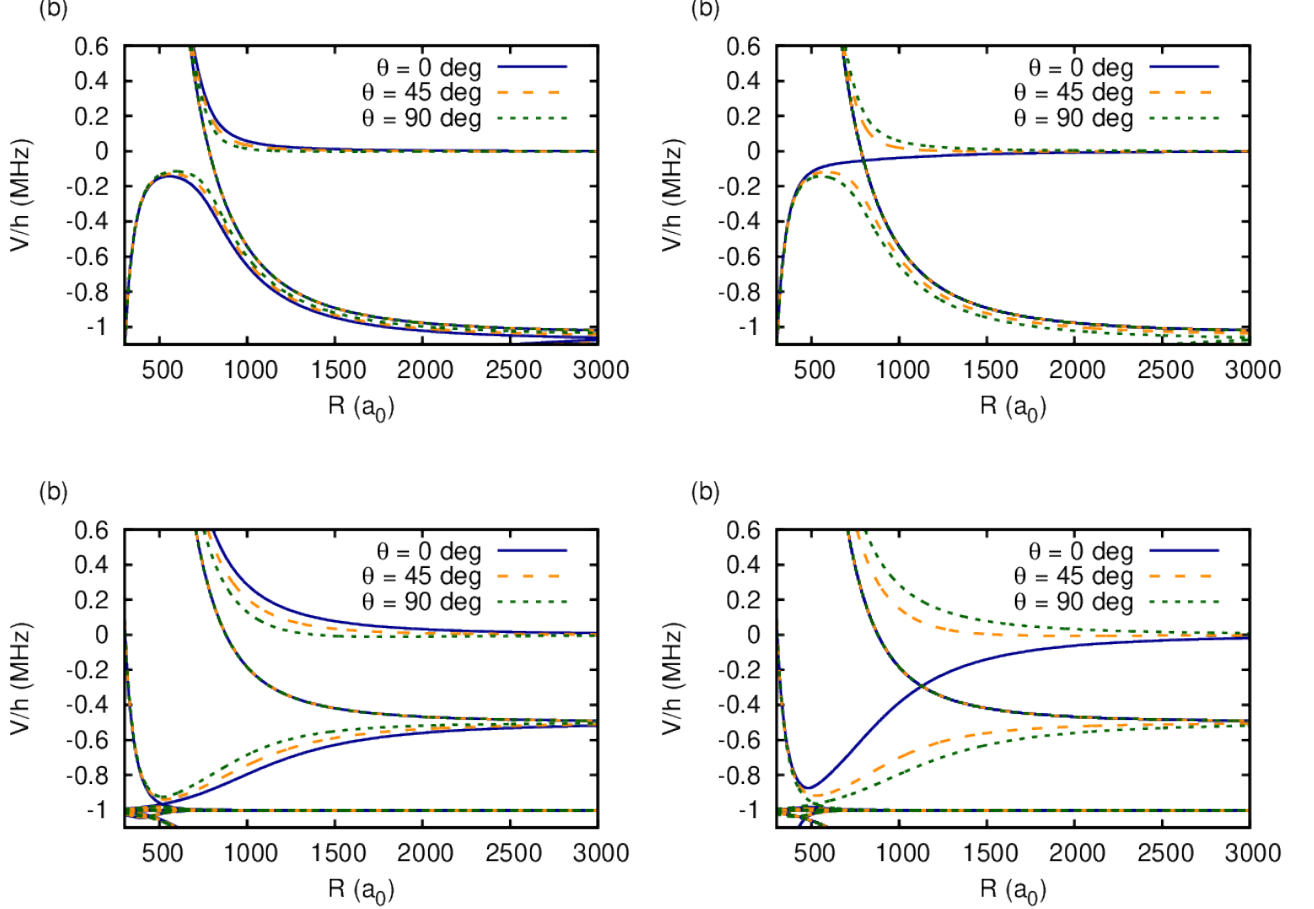


Figure 3. Adiabatic potential curves for RbCs+RbCs with $\Omega = 0.2$ MHz and fixed θ as indicated in the legend. The different panels correspond to: (a) Circular polarization for $\Omega \ll \Delta$, (b) linear polarization for $\Omega \ll \Delta$, (c) circular polarization for $\Omega \gg \Delta$, and (d) linear polarization for $\Omega \gg \Delta$.

is weakest and long-range space-fixed dipole-dipole interactions are attractive. For linear x polarization, shown in the center row, we find losses are also highest near $\theta = \pi/2$, where unshielded collisions along the polarization direction occur, as discussed above. These losses cannot be reduced by increasing the Rabi frequency. The bottom row shows results for elliptical polarization with $\xi = 0.2\pi/4$, which corresponds to 80 % pure circular polarization. The results are qualitatively similar to those in the case of circular polarization, but somewhat higher Rabi frequencies are required to suppress the loss.

V. CONCLUSIONS

We have investigated shielding of ultracold molecular collisions using microwave radiation with imperfectly circular polarization. The goal of microwave shielding is to prevent colliding pairs of molecules from reaching short range, where losses occur with high probability, while si-

multaneously avoiding long-range losses induced by the microwaves themselves. We have carried out coupled-channels calculations on RbCs+RbCs and CaF+CaF collisions to evaluate both the probabilities of reaching short range and the rate coefficients for microwave-induced loss.

We showed previously [19] that effective shielding can be achieved with circularly polarized microwaves but not with linearly polarized microwaves. However, pure circular polarization is hard to achieve in an apparatus designed for trapping ultracold molecules. Here we investigate how the effectiveness of shielding degrades for imperfectly circular polarization. We show that effective shielding can still be achieved with elliptical polarization that is around 90% circular.

Molecular fine and hyperfine structure can interfere with microwave shielding. We show that, for molecules in ${}^1\Sigma$ states, such as the bialkalies, effective shielding can be restored by applying a moderate magnetic field, of order 100 G, perpendicular to the plane of polarization.

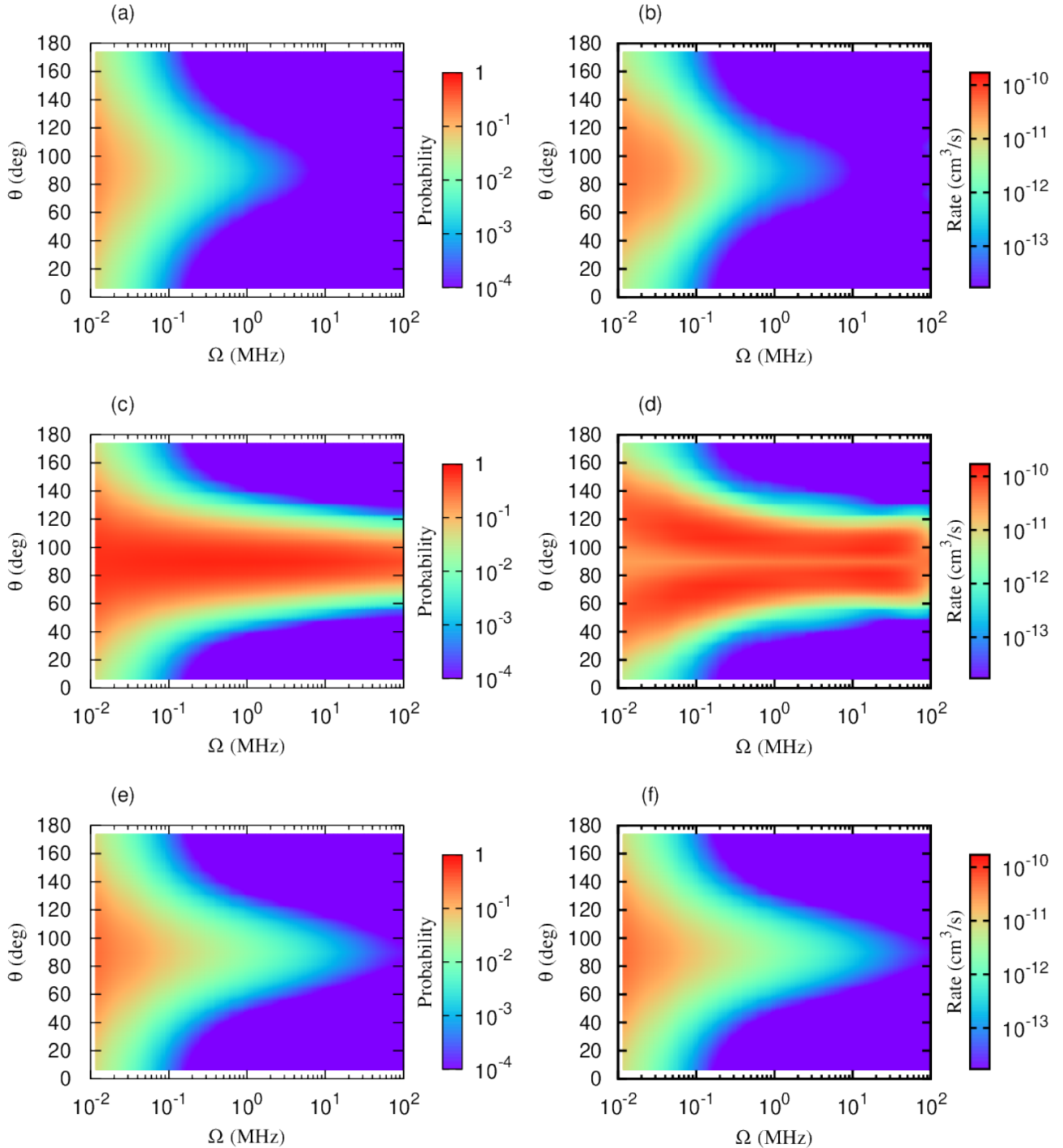


Figure 4. Probabilities for reaching short range [left-hand column, panels (a,c,e)] and rates of microwave-induced loss [right-hand column, panels (b,d,f)] as a function of Rabi frequency and fixed orientation θ . Panels (a,b) are for σ^+ circular polarization, (c,d) are for σ_x linear polarization, and panels (e,f) are for elliptical polarization with $\xi = 0.2\pi/4$.

For molecules in $^2\Sigma$ states, such as CaF, shielding is not fully restored by a magnetic field but losses can still be reduced by up to three orders of magnitude compared to the universal limit of complete short-range loss.

We interpret our results in terms of an approximate model in which collisions occur at a fixed orientation of the intermolecular axis. This simplifies the effective potential curves that govern shielding and loss. For linear

polarization, there are two curves in this model that cross (without an avoided crossing) when a collision occurs with the intermolecular axis along the axis of polarization. This is responsible for the lack of shielding for linear polarization. Elliptical polarization turns this crossing into an avoided crossing, which increases in strength as the degree of circular polarization increases. This restores effective shielding even for imperfectly circular polarization.

We anticipate that microwave shielding with near-

circular polarization will be a valuable tool for reducing collisional losses in samples of ultracold polar molecules.

VI. ACKNOWLEDGEMENT

This work was supported by the U.K. Engineering and Physical Sciences Research Council (EPSRC) Grants No. EP/P008275/1, EP/N007085/1 and EP/P01058X/1.

[1] S. Truppe, H. J. Williams, M. Hambach, L. Caldwell, N. J. Fitch, E. A. Hinds, B. E. Sauer, and M. R. Tarbutt, *Nature Physics* **13**, 1173 (2017).

[2] L. Anderegg, B. L. Augenbraun, Y. Bao, S. Burchesky, L. W. Cheuk, W. Ketterle, and J. M. Doyle, *Nature Physics* **14**, 890 (2018).

[3] K.-K. Ni, S. Ospelkaus, M. H. G. de Miranda, A. Pe'er, B. Neyenhuis, J. J. Zirbel, S. Kotochigova, P. S. Julienne, D. S. Jin, and J. Ye, *Science* **322**, 231 (2008).

[4] F. Lang, K. Winkler, C. Strauss, R. Grimm, and J. Hecker Denschlag, *Phys. Rev. Lett.* **101**, 133005 (2008).

[5] T. Takekoshi, L. Reichsöllner, A. Schindewolf, J. M. Hutson, C. R. Le Sueur, O. Dulieu, F. Ferlaino, R. Grimm, and H.-C. Nägerl, *Phys. Rev. Lett.* **113**, 205301 (2014).

[6] P. K. Molony, P. D. Gregory, Z. Ji, B. Lu, M. P. Köppinger, C. R. Le Sueur, C. L. Blackley, J. M. Hutson, and S. L. Cornish, *Phys. Rev. Lett.* **113**, 255301 (2014).

[7] J. W. Park, S. A. Will, and M. W. Zwierlein, *Phys. Rev. Lett.* **114**, 205302 (2015).

[8] M. Guo, B. Zhu, B. Lu, X. Ye, F. Wang, R. Vexiau, N. Bouloufa-Maafa, G. Quéméner, O. Dulieu, and D. Wang, *Phys. Rev. Lett.* **116**, 205303 (2016).

[9] T. M. Rvachov, H. Son, A. T. Sommer, S. Ebadi, J. J. Park, M. W. Zwierlein, W. Ketterle, and A. O. Jamison, *Phys. Rev. Lett.* **119**, 143001 (2017).

[10] F. Seefelberg, N. Buchheim, Z.-K. Lu, T. Schneider, X.-Y. Luo, E. Tiemann, I. Bloch, and C. Gohle, *Phys. Rev. A* **97**, 013405 (2018).

[11] S. Ospelkaus, K.-K. Ni, D. Wang, M. H. G. de Miranda, B. Neyenhuis, G. Quéméner, P. S. Julienne, J. L. Bohn, D. S. Jin, and J. Ye, *Science* **327**, 853 (2010).

[12] X. Ye, M. Guo, M. L. González-Martínez, G. Quéméner, and D. Wang, *Sci. Adv.* **4** (2018), 10.1126/sciadv.aaq0083.

[13] P. D. Gregory, M. D. Frye, J. A. Blackmore, E. M. Bridge, R. Sawant, J. M. Hutson, and S. L. Cornish, *Nature Comm.* **10**, 3104 (2019).

[14] P. S. Żuchowski and J. M. Hutson, *Phys. Rev. A* **81**, 060703(R) (2010).

[15] M. Mayle, G. Quéméner, B. P. Ruzic, and J. L. Bohn, *Phys. Rev. A* **87**, 012709 (2013).

[16] A. Christianen, T. Karman, and Groenenboom, (2019), arXiv:1905.06691.

[17] A. Christianen, M. W. Zwierlein, G. C. Groenenboom, and T. Karman, (2019), arXiv:1905.06846.

[18] A. V. Gorshkov, P. Rabl, G. Pupillo, A. Micheli, P. Zoller, M. D. Lukin, and H. P. Büchler, *Phys. Rev. Lett.* **101**, 073201 (2008).

[19] T. Karman and J. M. Hutson, *Phys. Rev. Lett.* **121**, 163401 (2018).

[20] B. R. Johnson, *J. Chem. Phys.* **69**, 4678 (1978).

[21] J. C. Light and A. Altenberger-Siczek, *J. Chem. Phys.* **64**, 1907 (1976).

[22] D. C. Clary and J. P. Henshaw, *Faraday Discuss. Chem. Soc.* **84**, 333 (1987).

[23] L. M. C. Janssen, A. van der Avoird, and G. C. Groenenboom, *Phys. Rev. Lett.* **110**, 063201 (2013).

[24] C. Cohen-Tannoudji, J. Dupont-Roc, and G. Grynberg, *Atom-Photon Interactions: Basic Processes and Applications* (Wiley, 1998).

[25] T. M. Hanna, E. Tiesinga, and P. S. Julienne, *New J. Phys.* **12**, 083031 (2010).

[26] D. J. Owens, T. Xie, and J. M. Hutson, *Phys. Rev. A* **94**, 023619 (2016).

[27] D. J. Owens and J. M. Hutson, *Phys. Rev. A* **96**, 042707 (2017).

[28] See supplement.

[29] Z. Idziaszek and P. S. Julienne, *Phys. Rev. Lett.* **104**, 113202 (2010).

[30] L. Lassablière and G. Quéméner, *Phys. Rev. Lett.* **121**, 163402 (2018).

**Supplementary Information for:
Microwave shielding of ultracold polar molecules
with imperfectly circular polarization**

Tijs Karman*, Jeremy M. Hutson

*Joint Quantum Centre (JQC) Durham-Newcastle, Department of Chemistry,
Durham University, South Road, Durham, DH1 3LE, United Kingdom*

**VII. SUPPRESSION OF THE EFFECTS OF
FINE AND HYPERFINE STRUCTURE BY
MAGNETIC FIELD**

Figure S1 shows rate coefficients for RSR (assuming 100% loss at short range) and microwave-induced loss for RbCs+RbCs collisions, including hyperfine structure, as a function of magnetic field perpendicular to the plane of circularly polarized microwave radiation. Results are shown for physical $^{87}\text{Rb}^{133}\text{Cs}$, as well as for RbCs with hyperfine interactions scaled up and down by a factor of three, respectively. The magnetic fields required to suppress the effect of hyperfine interactions are found also to increase and decrease by a factor three, respectively. The Zeeman interactions required to quantize the nuclear spins along the magnetic field are thus proportional to the magnetic field. This explains why suppression of the effects of fine and hyperfine structure was found to occur at approximately the same magnetic field, $B \approx 100$ G, for RbCs, KCs, and CaF. The hyperfine interactions are weaker for KCs than for RbCs, whereas for CaF the fine and hyperfine interactions are orders of magnitude stronger. However, the nuclear and electronic g -factors scale by approximately the same factors. Hence, the Zeeman interaction is weaker (stronger) for KCs (CaF) by approximately the same factor, such that similar magnetic fields provide suppression of the effects of hyperfine interactions in the three systems.

In the low-field limit, the enhancement of microwave-induced loss due to fine and hyperfine interactions also increases with the strength of the hyperfine interactions, as can be seen in Fig. S1. This is also in line with Ref. [19], where it was found that the enhancement of microwave-induced loss is smaller for KCs than for RbCs, and much larger for CaF than for RbCs.

In the high-field limit, the fine and hyperfine enhancement of microwave-induced loss is suppressed because the spins quantize along the magnetic field. The spin projections effectively become spectator quantum numbers, and only the initial spin state contributes. Fine and hyperfine terms averaged over this spin state do exist, although they are not present in the spin-free calculation. For example, for a spin $|SM_S\rangle$ along the magnetic field axis, the spin-rotation interaction, $\gamma \hat{N} \cdot \hat{S}$, is averaged to a term $\langle SM_S | \gamma \hat{N} \cdot \hat{S} | SM_S \rangle = \gamma M_S \hat{N}_z$, which does not occur in the spin-free case. For the bialkalies

RbCs and KCs, $\gamma \ll \Omega$. The averaged hyperfine terms can thus be neglected and the loss rates are suppressed

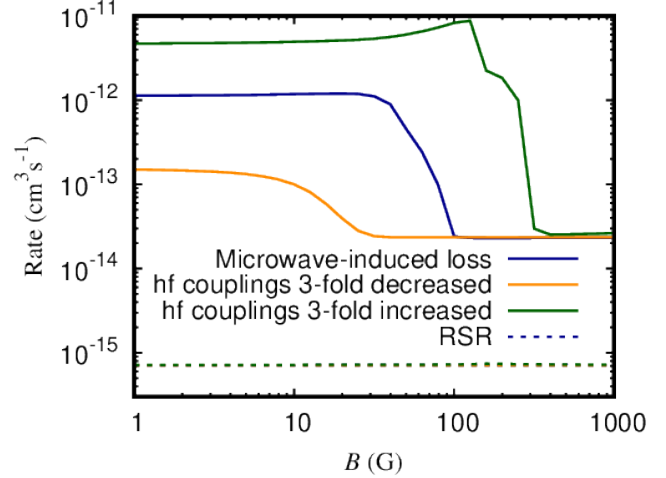


Figure S1. Rate coefficients for RSR and microwave-induced loss in RbCs+RbCs collisions, as a function of the magnetic field strength, B . The loss rates shown are obtained using the physical hyperfine constants, as well as hyperfine constants scaled up or down by a factor 3. For scaled hyperfine interactions, the suppression occurs at approximately $B = 30$ G and 300 G, rather than 100 G. The effect of hyperfine interactions on the microwave-induced loss rate also scales with the magnitude of the hyperfine coupling constants.

to the hyperfine-free level. For CaF, however, the fine and hyperfine interactions are not negligible compared to $\Omega = 100$ MHz; for example, the electron-spin-rotation constant is $\gamma \approx 40$ MHz. The effect of the spin-averaged terms is significant: Loss rates for CaF+CaF as a function of magnetic field for $\Omega = 100$ MHz are shown in Fig. S2. For high magnetic fields, the microwave-induced loss approaches a constant that is significantly higher than the spin-free loss rate. This figure also includes the loss rates obtained by averaging over a single spin-stretched state; they agree quantitatively with the high-field results from full calculations including all fine and hyperfine states. This again illustrates that the suppression of fine and hyperfine interactions results from uncoupling of the spin and rotational degrees of freedom by quantizing the spins along the external magnetic field axis.

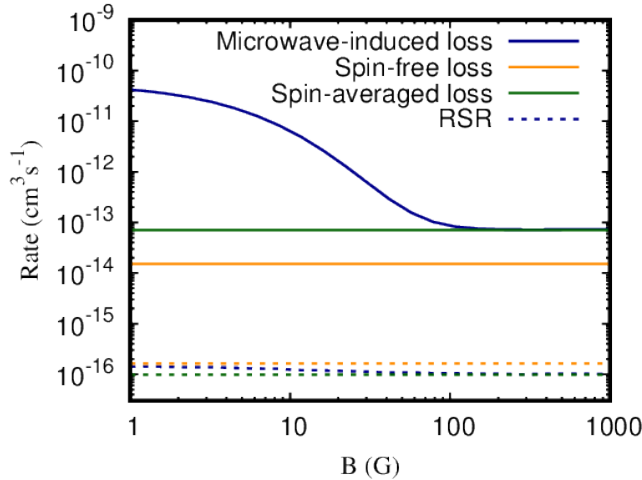


Figure S2. Rate coefficients for RSR and microwave-induced loss in $\text{CaF} + \text{CaF}$ collisions, as a function of the magnetic field strength, B . Loss rates shown are obtained from three sets of calculations: A full calculation that includes the fine and hyperfine structure, a spin-free calculation that neglects fine and hyperfine interactions altogether, and a spin-averaged calculation in which fine and hyperfine interactions are averaged over the spin-stretched initial hyperfine state.